Geophysical Research Letters

RESEARCH LETTER
10.1029/2025GL116146

Radial Rainfall Pattern Changes of Intense Over-Ocean Tropical Cyclones Under Global Warming: Insights From an MRI HighRes CMIP6 Simulation

Jianan Chen[1], Ralf Toumi[2], Lujia Zhang[3], Mengqian Lu[3], Dazhi Xi[1], and Xiaoming Shi[4,5]

[1]Department of Earth Sciences, University of Hong Kong, Hong Kong, China, [2]Department of Physics, Imperial College London, London, UK, [3]Department of Civil and Environmental Engineering, Hong Kong University of Science and Technology, Hong Kong, China, [4]Division of Environment and Sustainability, Hong Kong University of Science and Technology, Hong Kong, China, [5]Center for Ocean Research in Hong Kong and Macau, Hong Kong University of Science and Technology, Hong Kong, China

Key Points:

- The tropical cyclone (TC) maximum rainfall increases by about 8.65%/K and the spatial extent of the rainfall slightly decreases by about 1.79%/K
- The TC maximum rainfall strongly correlates with a moisture convergence proxy
- The proxy is the maximum wind at the top of the boundary layer times the column water vapor divided by the radius of maximum wind

Supporting Information:

Supporting Information may be found in the online version of this article.

Correspondence to:

X. Shi,
shixm@ust.hk

Citation:

Chen, J., Toumi, R., Zhang, L., Lu, M., Xi, D., & Shi, X. (2025). Radial rainfall pattern changes of intense over-ocean tropical cyclones under global warming: Insights from an MRI HighRes CMIP6 simulation. *Geophysical Research Letters*, *52*, e2025GL116146. https://doi.org/10.1029/2025GL116146

Received 28 MAR 2025
Accepted 24 APR 2025

Author Contributions:

Conceptualization: Jianan Chen
Data curation: Jianan Chen
Formal analysis: Jianan Chen, Lujia Zhang, Mengqian Lu, Xiaoming Shi
Funding acquisition: Mengqian Lu, Dazhi Xi, Xiaoming Shi
Investigation: Jianan Chen, Xiaoming Shi
Methodology: Jianan Chen, Ralf Toumi
Project administration: Ralf Toumi, Xiaoming Shi
Software: Jianan Chen, Lujia Zhang
Supervision: Ralf Toumi, Xiaoming Shi
Validation: Jianan Chen
Visualization: Jianan Chen
Writing – original draft: Jianan Chen

Abstract Tropical cyclone (TC) rainfall is an important hazard. Radial rainfall patterns of intense over-ocean TCs under global warming are investigated using the MRI HighRes Coupled Model Intercomparison Project Phase 6 simulation with the SSP5-8.5 high-emission scenario. These patterns are characterized by four parameters: rainfall at the cyclone center (T_o), maximum rainfall (T_m), radius of maximum rainfall (R_m), and e-folding radius (R_e). We find T_m strongly correlates $(r = 0.8)$ with a moisture convergence proxy—boundary-layer maximum wind times column moisture divided by the radius of maximum wind—across different intensities and under climate change. Under warming, mean T_m and T_o increase by 8.65%/K and 8.86%/K, while R_m and R_e shrink by 1.03%/K and 1.79%/K, respectively. Notably, under warming, T_m exhibits greater sensitivity to TC intensity, and its increases are mainly attributed to column moisture increase.

Plain Language Summary Tropical cyclones can bring heavy rainfall, which poses significant risks to communities. In this study, we looked at how rainfall is distributed around a cyclone using four key measurements: the rainfall at the center of the cyclone, the maximum rainfall, the distance from the center to where the maximum rainfall occurs, and how quickly the rainfall decreases with distance. We found that the maximum rainfall is closely related to a combination of the storm's wind speed and the amount of moisture in the atmosphere, divided by the distance to where the maximum wind occurs. This relationship remains consistent even in a warmer climate. We also found that as the climate warms, the maximum rainfall amount increases by about 8%–9% per degree of warming mainly due to increased moisture in the atmosphere. The areas where the intense rainfall occurs shrink slightly, suggesting more compacted rainfall patterns under warming.

1. Introduction

Tropical cyclones (TC) can bring heavy and persistent precipitation over several days during their passages, inducing devastating flash floods and landslides that cause enormous societal and economic losses (Knutson et al., 2020; Liu et al., 2019). Given the ongoing rise in global temperatures resulting from greenhouse gas emissions, there is considerable interest in understanding future changes in TC precipitation (Shi et al., 2024). With ongoing advancements in computational power, cutting-edge high-resolution General Circulation Models (GCMs) have emerged, markedly enhancing the simulation of global TC activity and their structural characteristics (Roberts et al., 2020). In this study, we utilize the MRI HighRes simulation from the Coupled Model Intercomparison Project Phase 6 (CMIP6) High Resolution Model Intercomparison Project (HighResMIP), which features a horizontal grid resolution as fine as 25 km, a significant improvement over traditional GCMs that typically use coarser grids of hundreds of kilometers. We chose this simulation for its extended simulation period (2015–2099) under the high-emission SSP5-8.5 scenario, which projects pronounced warming and distinguishes anthropogenic climate change signals from natural internal variability, enabling a more precise analysis of global TC rainfall pattern changes under warming.

The radial distribution of TC rainfall is a fundamental metric in characterizing the TC rainfall. This distribution can be described by (Lonfat et al., 2004),

Writing – review & editing: Jianan Chen, Ralf Toumi, Lujia Zhang, Dazhi Xi

$$P_{\mathrm{sym}} = \begin{cases} T_o + (T_m - T_o)\left(\dfrac{R}{R_m}\right), & \text{if } R < R_m \\ T_m \exp\left(\dfrac{R_m - R}{R_e}\right), & \text{if } R \geq R_m \end{cases} \tag{1}$$

where T_o is the rain rate at the center of the TC, T_m is the maximum rain rate in the radial profile of TC rainfall, R_m is the radius of the maximum rain rate, and R_e is the e-folding radius of the maximum rain rate, measuring the spatial decay rates of TC rainfall from T_m outward from the center (e.g., Kim et al., 2022; Lonfat et al., 2004). In real-world TCs, the eye typically lacks rainfall (e.g., Emanuel, 2018), but T_o is a relevant variable in this study because the 25 km resolution of the MRI HighRes CMIP6 simulation cannot resolve TC eyes, leading to modeled rainfall at the center. Additionally, R_e reflects the spatial extent of TC rainfall (Tuleya et al., 2007). The rainfall intensifies linearly with radius from the cyclone center up to R_m and then declines exponentially. In previous studies (e.g., Stansfield & Reed, 2023), the TC radial rainfall pattern for a certain climate period is described by the mean TC radial rainfall profile, which is often derived by averaging multiple radial rainfall profiles. The mean TC rainfall profiles are then compared between different climate periods to describe the changes in the TC radial rainfall pattern. However, the changes in the four rainfall distribution parameters (T_m, T_o, R_e, and R_m) are often overlooked and underinterpreted, despite being critical for explaining the underlying causes of radial rainfall profile changes. Unlike prior work, our study uniquely targets these parameters to provide a detailed physical understanding of TC rainfall changes under warming.

In this study, we aim to investigate changes in TC radial rainfall pattern using the MRI HighRes CMIP6 simulation, examining how T_m, T_o, R_e, and R_m evolve under warming. By reassessing the TC wind-rain relationships within this climate data set, we identify the primary drivers of T_m, T_o, R_e, and R_m and develop an improved parametric rainfall model, to better interpret their changes under warming. Our analysis focuses on individual TC snapshots, with an emphasis on intense over-ocean TCs due to their greater destructive potential and well-preserved structures compared to weaker TCs or those disrupted by landfall.

2. Methods

2.1. Data

The data (Mizuta et al., 2019) comes from a high-resolution climate simulation provided by the HighResMIP, which is part of the CMIP6. This simulation was conducted using Japan's Meteorological Research Institute–Atmospheric GCM version 3.2 (MRI-AGCM-M3-2), a model with a horizontal grid resolution of 25 km. The simulation belongs to HighResMIP's “highresSST-future” experiments. In this setup, the model is forced with pre-set sea surface temperatures (SSTs) based on a high-emission scenario (SSP5-8.5), which projects a future with significant global warming. By using these fixed future SSTs, the model focuses solely on atmospheric responses to warmer oceans without simulating interactive ocean dynamics. This product is known for its capability in simulating strong TCs (Roberts et al., 2020). It differs from other HighResMIP products due to its extended simulation period, being the only or one of few data sets providing continuous simulation from 2015 to 2099 with 25 km horizontal grid resolution. The product is available at daily time intervals.

2.2. TC Tracking and Metrics

TempestExtremes software package is used to track TCs based on daily output from the MRI HighRes CMIP6 simulation (Ullrich et al., 2021). This TC tracking algorithm identifies cyclones by detecting a nearby sea-level pressure minimum coinciding with an upper-level warm core, with key parameters following the TC tracking approach for ERA5 described by Ullrich et al. (2021). TC searching is restricted to 30°S–30°N to exclude samples undergoing extratropical cyclone transition. Detailed command lines used for tracking are provided in Table S1 in Supporting Information S1. Cyclones are classified into landfall and over-ocean TCs based on whether their low-pressure centers are within 300 km of the coastline; this study focuses exclusively on over-ocean TCs. TC snapshots are further categorized by intensity ($V_{\max_{10m}}$), derived from the 10 m wind speed output from the model, into tropical storm (TS, CAT0, 17–33 m/s) and Categories 1–5 (CAT1–CAT5) using the Saffir–Simpson Hurricane Wind Scale.

Two climate periods are examined: the present climate (2015–2034) and the future climate (2080–2099). In the present climate, TempestExtremes identified 6,524 TC snapshots, distributed as follows: 3,677 TS, 1,006 CAT1, 452 CAT2, 423 CAT3, 691 CAT4, and 275 CAT5. For the future climate, 5,242 snapshots were identified, with a distribution of 2,620 TS, 702 CAT1, 365 CAT2, 427 CAT3, 751 CAT4, and 377 CAT5. Intense TCs in this study refer to snapshots reaching at least CAT3. We compared them with observations from the International Best Track Archive for Climate Stewardship (IBTrACS, Knapp et al. (2010)) over 2005–2024, processed to daily frequency to match the MRI data. IBTrACS yields 7,803 snapshots: 4,941 TS, 1,241 CAT1, 629 CAT2, 448 CAT3, 444 CAT4, and 100 CAT5. Relative to IBTrACS, the present climate simulation underestimates TS and CAT1–CAT3 frequencies (e.g., 3,677 vs. 4,941 for TS) but overestimates CAT4 (691 vs. 444) and CAT5 (275 vs. 100), suggesting a bias toward higher intensities. In the future climate, the 5,242 snapshots show a marked decrease in TS frequency (2,620) and increases in CAT4 (751) and CAT5 (377), indicating a shift toward more intense TCs, consistent with warming projections (Knutson et al., 2020).

2.3. TC Rainfall Parametric Models

2.3.1. PHRaMM

The physical drivers that cause the change of the four rainfall distribution parameters are simply assumed to be TC intensity (Lonfat et al., 2007; Tuleya et al., 2007) and atmospheric moisture (Kim et al., 2022). In Parametric Hurricane Rainfall Model with moisture (PHRaMM), the prediction of the four rainfall distribution parameters is based on multiple linear regression using $V_{\max_{10m}}$ and total column water vapor (TCW) as independent explanatory variables (Kim et al., 2022).

$$T'_m = a_1 + b_1 * V_{\max_{10m}} + c_1 * TCW, \tag{2a}$$

$$T'_o = a_2 + b_2 * V_{\max_{10m}} + c_2 * TCW, \tag{2b}$$

$$R'_e = a_3 + b_3 * V_{\max_{10m}} + c_3 * TCW, \tag{2c}$$

$$R'_m = a_4 + b_4 * V_{\max_{10m}} + c_4 * TCW, \tag{2d}$$

where the T'_m, T'_o, R'_e, and R'_m are fitted values. Hereafter, we use this primed notation (T'_m, T'_o, R'_e, R'_m) to represent fitted values, while T_m, T_o, R_e, and R_m refer to the actual values derived from radial rainfall profiles in the climate data set. Following He et al. (2022), total column water vapor is calculated by,

$$\int_{surface}^{top} q \frac{dp}{g}, \tag{3}$$

where q is the specific humidity, g is the gravitational constant and dp represents the pressure difference between different model levels. Unlike Kim et al. (2022) where TCW is derived based on conditions during the storm, the TCW in this study is calculated based on the monthly mean of total column water vapor at the location of the storm. The monthly mean TCW representing persistent background moisture conditions, yields a clearer signal of the climatic drivers of rainfall, as opposed to the day-to-day TCW affected by the storm itself. Unlike TCW, which is monthly averaged, the other variables in this study are not monthly averaged to capture TC-specific dynamics.

The primary limitation of PHRaMM lies in its low correlation between the fitted rainfall distribution parameters (e.g., T_m) and the observed one (see Table 1 in Kim et al. (2022)), suggesting its low capacity in capturing the TC rainfall field variability.

2.3.2. PHRaM_S

Motivated by better capturing the TC rainfall field variability, the parametric hurricane rainfall model for symmetric component (PHRaM_S) is developed by exploring the TC wind-rain relationship in the MRI HighRes CMIP6 climate data set. Predictor variables for PHRaM_S were selected through a combination of correlation analysis and physical reasoning (detailed in Section 4), prioritizing those with the strongest correlations to each rainfall distribution parameter. For T_m and T_o, we used $TCW\frac{V_{\max_{850}}}{R_{\mathrm{mw}_{850}}}$ —where $V_{\max_{850}}$ and $R_{\mathrm{mw}_{850}}$ represent the

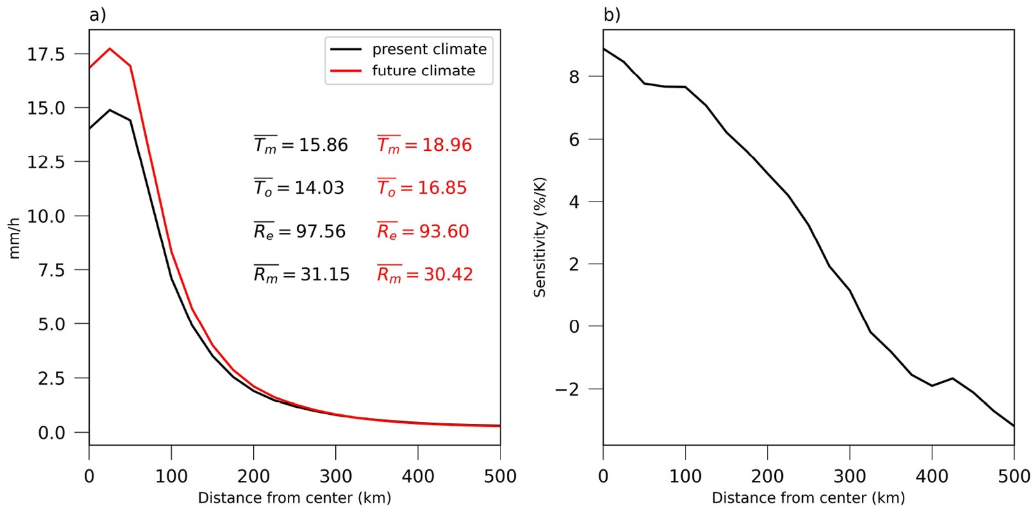

Figure 1. The rainfall radial distribution (a) of over-ocean TCs (Category 3 and above) and the corresponding sensitivity per degree of warming (b). The mean T_m (mm/hr), T_o (mm/hr), R_e (km), and R_m (km) are listed in panel (a). The text in black font indicates values for the current climate period, while the text in red font represents values for the future climate period.

maximum wind and radius of maximum wind at 850 hPa—because it captures moisture convergence, the key driver of inner-core rainfall, by combining moisture (TCW) and convergence $\left(\frac{V_{\max_{850}}}{R_{\mathrm{mw}_{850}}}\right)$. For R_e and R_m, we related them to $R_{\mathrm{mw}_{850}}$ and $V_{\max_{850}}$, respectively, as correlation analysis showed these variables correlate better than TCW or $V_{\max_{10m}}$.

$$T'_m = a_1 + b_1 \left(TCW \frac{V_{\max_{850}}}{R_{\mathrm{mw}_{850}}}\right), \tag{4a}$$

$$T'_o = a_2 + b_2 \left(TCW \frac{V_{\max_{850}}}{R_{\mathrm{mw}_{850}}}\right), \tag{4b}$$

$$R'_e = a_3 + b_3 \left(R_{\mathrm{mw}_{850}}\right), \tag{4c}$$

$$R'_m = a_4 + b_4 \left(V_{\max_{850}}\right). \tag{4d}$$

3. Radial Rainfall Patterns

The traditional approach to understanding the TC radial rainfall pattern changes under warming involves analyzing the mean TC radial rainfall profiles. Figure 1a presents the mean radial rainfall profiles of intense over-ocean TCs for the present and future climates. These profiles are derived by averaging multiple profiles of over-ocean TC snapshots that reach at least Category 3. The radial rainfall profiles exhibit a maximum near the cyclone center at 25 km for both climate periods. The maximum rainfall T_m decreases exponentially with increasing distance from the cyclone center. Additionally, the rainfall at the center is slightly smaller than the radial rainfall maximum, suggesting that the TC eyewall is not well resolved. In the future climate, the mean SST increases by 2.26 K relative to the present climate. The corresponding precipitation sensitivity is shown in Figure 1b. The TC rainfall shows super Clausius-Clapeyron (C-C) scaling at the center and negative sensitivity at the TC outer region (beyond 325 km). These results contrast with recent observation-based studies (e.g., Tu et al., 2021) that suggest decreasing inner core precipitation and enhanced outer rainband precipitation in the recent two decades. However, the super C-C scaling in the inner core is consistent with many modeling-based studies (e.g., Liu et al., 2019). The discrepancy with Tu et al. (2021) may arise from their analysis of a shorter, modestly warming period (0.5°C from 1999 to 2018), where trends could be influenced by natural variability or over-land TCs. While much is known about how radial rainfall patterns change, the underlying causes of these shifts remain unclear.

This study seeks to explore the underlying causes of the radial rainfall pattern shifts under warming by examining changes in T_m, T_o, R_e, and R_m. The mean values of these parameters—denoted as $\overline{T_m}$, $\overline{T_o}$, $\overline{R_e}$, and $\overline{R_m}$—for the present and future climates are presented in Figure 1a. Notably, these mean parameter values differ from those inferred directly from the mean radial profile in Figure 1a. For instance, T_m in the present climate based on the mean profile is 14.88 mm/hr, whereas the $\overline{T_m}$ is slightly larger at 15.86 mm/hr. This difference occurs because, in the mean radial profile, the averaging over different profiles smooths out T_m. Relative to the present climate, the $\overline{T_m}$ and $\overline{T_o}$ increase by 19.54% (8.65%/K) and 20.09% (8.86%/K) respectively, in the future climate. The $\overline{R_m}$ shows a slight decrease from 31.15 to 30.42 km. Considering R_m is in the grid size of 25 km, the slight change in R_m is probably due to the model's inability to capture its variation. The $\overline{R_e}$ decreases by 4.05% (1.79%/K) in the future climate. The shrinking $\overline{R_e}$ under warming indicates a faster decay of rainfall from the radial maximum under warming. The decreased rainfall in the TC outer region under warming (Figure 1) is likely related to this faster decay.

4. TC Wind-Rain Relationships

In this section, we investigate the relationships between TC wind and rainfall within the MRI climate data set to elucidate the physical drivers of the radial rainfall parameters: T_m, T_o, R_m, and R_e. Our objectives are twofold: first, to identify the key factors controlling changes in T_m, T_o, R_m, and R_e under warming conditions; and second, to leverage the most influential drivers to construct the PHRaM_S.

The inner core precipitation has been found to be positively correlated with TC intensity measured by the surface wind maximum $V_{\max_{10m}}$ (e.g., Xi & Lin, 2022; Xi et al., 2022). Figure 2a shows the correlation coefficients (r) between T_m and explanatory variables for TC snapshots that reach CATn (where n ranges from 0 to 5). T_m shows low correlations with $V_{\max_{10m}}$ within individual category groups. Figure 2b shows the same relationships except for TC snapshots that reach at least CATn. Unlike Figure 2a, T_m shows high correlations with $V_{\max_{10m}}$ when all TCs, including CAT0 tropical storms, are considered. As weaker TCs are increasingly excluded, the correlation between $V_{\max_{10m}}$ and T_m drops (Figure 2b), which is probably related to decreased variabilities in $V_{\max_{10m}}$. If only intense TCs (CAT3+) are considered, the correlation coefficient drops to 0.39. In contrast, $V_{\max_{850}}$ shows a much stronger correlation with T_m (Figures 2a and 2b) and maintains a high correlation even for the strongest portion of TCs. Although $V_{\max_{850}}$ and $V_{\max_{10m}}$ are often assumed to be highly correlated, we found a decline in correlation between $V_{\max_{850}}$ and $V_{\max_{10m}}$ as weaker TCs are increasingly excluded (Figure 2c). Compared to the surface level where the circulation is affected by surface friction, the TC circulation is arguably better represented by the 850 hPa level, which is approximately at the top of the hurricane boundary layer and less affected by surface friction.

The moisture convergence into the TC center drives the upward moisture flux and creates convective precipitation near the cyclone center (Liu et al., 2019). Assuming the radial inflow velocity (V_r) is proportional to the maximum wind ($Vmax$) at the radius of maximum wind (Rmw) and V_r is zero near the TC center, the radial convergence $\frac{V_r}{R_{\mathrm{mw}}}$ is proportional to $\frac{V_{\max}}{R_{\mathrm{mw}}}$. Considering the environmental moisture, the moisture convergence into the TC can therefore be related to $TCW\,\frac{V_{\max}}{R_{\mathrm{mw}}}$. In our climate simulation data set, T_m is found to be positively related to TCW, negatively related to $R_{\mathrm{mw}_{850}}$, and positively related to $V_{\max_{850}}$ (Figures 2a and 2b). These relationships are consistent with previous studies that suggest increased moisture (Kim et al., 2022), a shrinking radius of maximum wind (Yu et al., 2022), and stronger TC intensity (Tuleya et al., 2007) correspond to an enhanced radial rainfall maximum. The moisture convergence proxy, $TCW\,\frac{V_{\max_{850}}}{R_{\mathrm{mw}_{850}}}$, is strongly correlated with T_m (Figures 2a and 2b) and is used to predict T'_m in the PHRaM_S. The PHRaMM serves as the benchmark model. The performance of PHRaM_S and PHRaMM in predicting T_m is evaluated using correlation coefficients between the fitted T'_m and the actual T_m derived from radial rainfall profiles in the climate data set. For intense TCs (CAT3+), PHRaMM's correlation coefficient declines sharply (Figure 2d), whereas PHRaM_S remains stable, consistently achieving higher correlation coefficients across these strong storms.

T_o, rainfall at TC center, shares a similar correlation analysis with T_m (Figures S1a, S1b, and S1d in Supporting Information S1). T_o is strongly correlated with T_m (Figure S1c in Supporting Information S1) because the inner core is not well resolved in the 25-km resolution GCM simulation. However, $TCW\,\frac{V_{\max_{850}}}{R_{\mathrm{mw}_{850}}}$ correlates less strongly

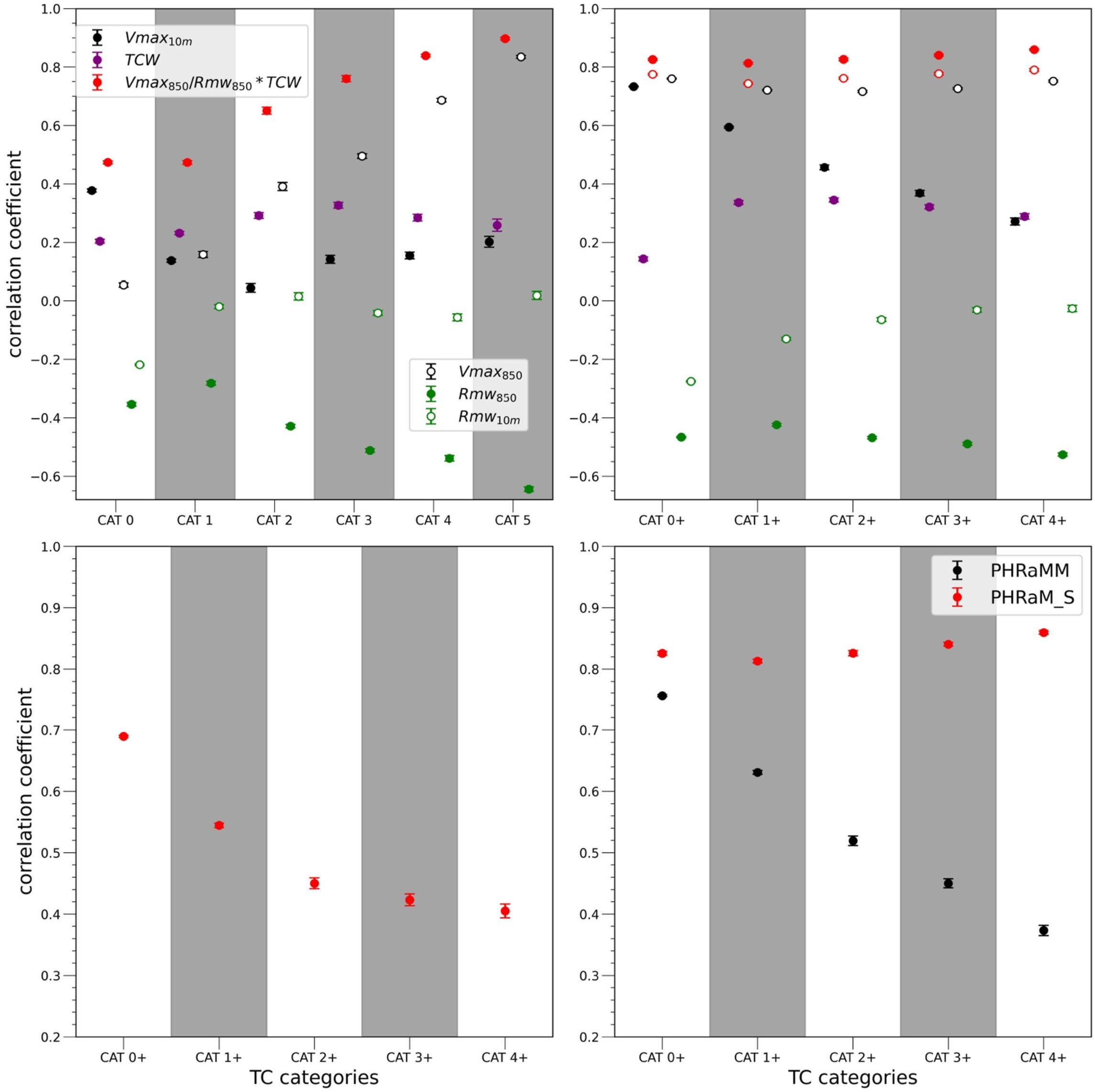

Figure 2. (a) The correlation coefficients between explanatory variables and T_m for CAT0, CAT1, CAT2, CAT3, CAT4, and CAT5 TCs. (b) Same as (a), except for CATn+ TCs. The term CATn+ refers to the tropical cyclone snapshots that reach at least CATn, where n ranges from 0 to 4. (c) The correlation coefficients between $V_{\max}$ at the surface ($V_{\max_{10m}}$) and $V_{\max}$ at 850 hPa ($V_{\max_{850}}$) for CATn+ TCs. (d): The correlation coefficients between T_m and T_{fm} from Parametric Hurricane Rainfall Model with moisture and PHRaM_S. The error bar represents the standard deviation of correlation coefficients across the ten models generated using a leave-one-out cross-validation subsampling method, as described by Kim et al. (2022). All depicted correlations meet the $p < 0.05$ threshold.

with T_o than with T_m (Figure 2 and Figure S1 in Supporting Information S1), probably because subsidence or other processes also influence precipitation at the center of the TC.

R_e, the e-folding radius, measures the rainfall spatial extent. Kim et al. (2022) reported that R_e is negatively correlated with $V_{\max_{10m}}$, which we confirm when all TCs are included (Figure 3a). However, the negative correlation weakens and turns slightly positive for very intense TCs (e.g., CAT4+). Therefore, $V_{\max_{10m}}$ is not a robust explanatory variable accounting for R_e change. $V_{\max_{850}}$ shows a more consistent, though still weak, negative correlation (Figure 3a), while TCW's weak correlation suggests minimal influence from environmental moisture. Yu et al. (2022) linked the TC rainfall distribution to TC sizes. Accordingly, we investigate the correlation between R_e and TC sizes. The TC out core sizes are measured by the radius of gale-force wind, R_{17}. The TC inner-core sizes are measured by the radius of maximum wind. Both R_{17} at the surface and 850 hPa are positively

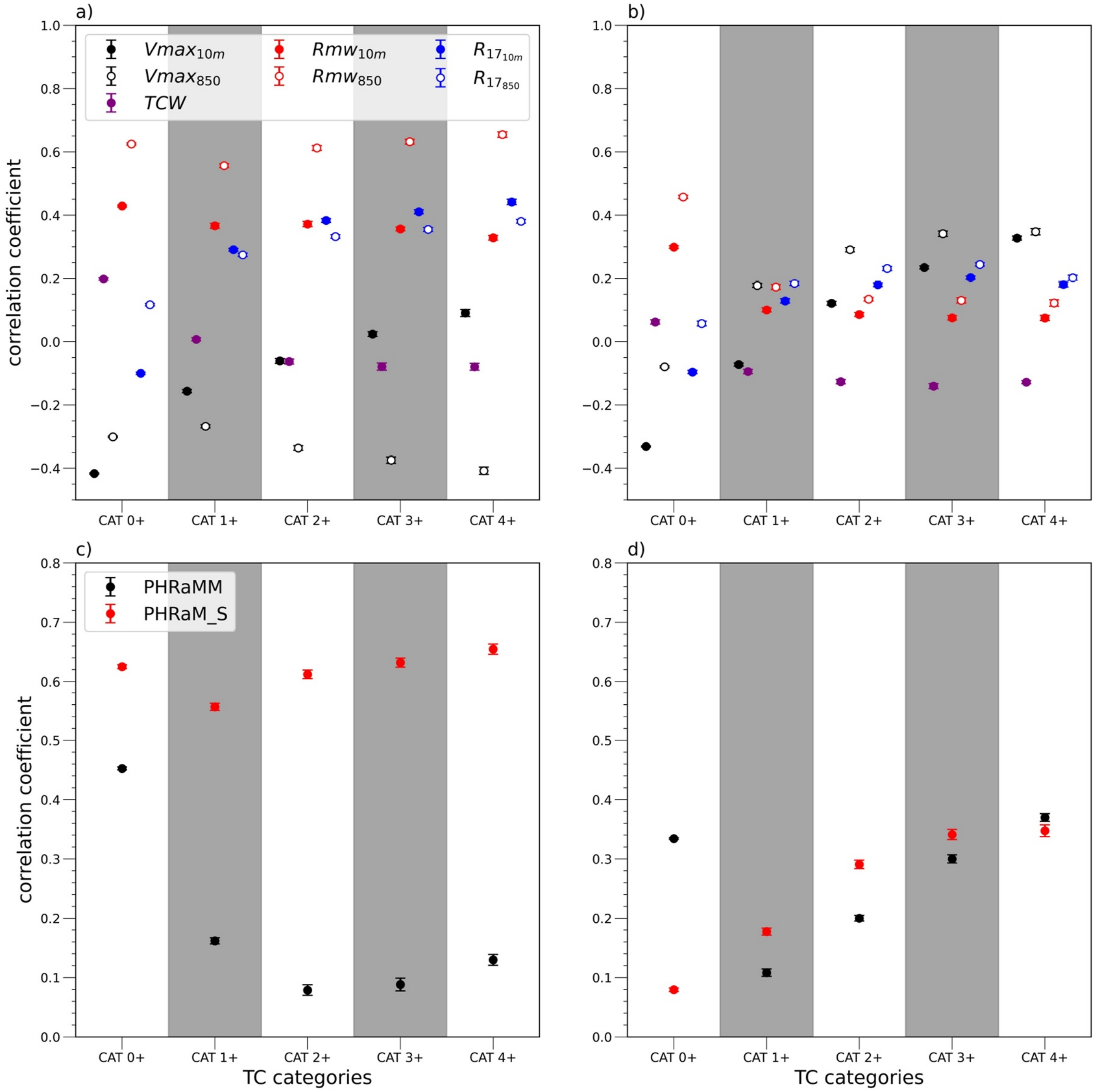

Figure 3. (a) The correlation coefficients between explanatory variables and R_e for CATn+ TCs. (b) Same with (a) except for R_m. (c) The correlation coefficients between R_e and R_e' from Parametric Hurricane Rainfall Model with moisture and PHRaM_S. (d) Same as (c) except for R_m and R_m'. The CATn+ TCs means instant tropical cyclone samples that reach at least CATn, where n ranges from 0 to 4. The error bar represents the standard deviation of correlation coefficients across the ten models generated using a leave-one-out cross-validation subsampling method, as described by Kim et al. (2022). All depicted correlations meet the $p < 0.05$ threshold.

correlated with R_e. $R_{\mathrm{mw}_{850}}$ has the strongest positive correlation with R_e across subsets of TCs, indicating that a larger inner core corresponds to a slower spatial decay of the radial rainfall maximum. $R_{\mathrm{mw}_{850}}$ is therefore selected as predictor in PHRaM_S. The simple linear regression is adopted because we found a multiple linear regression model using additional variables such as environmental moisture leads to high model uncertainties, with regressed coefficients changing significantly when different subset samples are used to train the model. Nevertheless, the PHRaM_S shows significantly higher correlation coefficients than the PHRaMM (Figure 3c).

R_m, the radius of maximum rainfall, shows weak correlations with TC size, wind speed, and moisture (Figure 3b). The correlation with $V_{\max_{10m}}$ ($V_{\max_{850}}$) shifts from negative to positive as weaker TCs are excluded, contrasting with observational studies reporting a negative trend (e.g., Kim et al., 2022; Lonfat et al., 2004). This discrepancy may stem from their inclusion of tropical storms, inflating R_m differences, or from unrealistic wind-rain relationships in our 25 km resolution model, which struggles to resolve eyewall structures (Shi et al., 2024). For

Table 1
The Intercepts, Regression Coefficients for T_m, T_o, R_e, and R_m Using PHRaM_S, and Correlation Coefficient Between Fitted and Actual Parameters

Parameter	Intercept	Slope	Corr. Coeff.
(a) Present climate			
T_m	a_1 = 6.63 (0.10)	b_1 = 0.77 (0.010)	0.82 (0.0056)
T_o	a_2 = 7.31 (0.17)	b_2 = 0.56 (0.014)	0.65 (0.0078)
R_e	a_3 = 46.81 (1.37)	b_3 = 0.37 (0.013)	0.64 (0.0079)
R_m	a_4 = 11.57 (0.65)	b_4 = 0.70 (0.021)	0.30 (0.0108)
(b) Future climate			
T_m	a_1 = 7.03 (0.09)	b_1 = 0.79 (0.006)	0.84 (0.0065)
T_o	a_2 = 7.84 (0.17)	b_2 = 0.61 (0.013)	0.69 (0.0098)
R_e	a_3 = 47.44 (1.45)	b_3 = 0.35 (0.014)	0.62 (0.0116)
R_m	a_4 = 7.93 (0.68)	b_4 = 0.79 (0.020)	0.37 (0.0113)

Note. Data are from ocean TC snapshots reaching at least category 3. The upper panel represents the present climate, and the lower panel represents the future climate. Parentheses denote the standard deviation of each coefficient across ten models, derived from ten subsampling groups using the leave-one-out cross-validation method (Kim et al., 2022). Units for a_1, a_2, a_3, and a_4 are mm/hr, mm/hr, km, and km, respectively; units for b_1, b_2, b_3, and b_4 are m^3/kg, m^3/kg, km/km, and s, respectively.

intense TCs (CAT3+), $V_{\max_{850}}$ offers the strongest correlation with R_m (Figure 3b) and is used in PHRaM_S (Figure 3d), again favoring simple regression due to coefficient instability in multiple regression.

5. Rainfall Pattern Change Interpretation

The PHRaM_S is used to interpret the changes in $\overline{T_m}$, $\overline{T_o}$, $\overline{R_e}$, and $\overline{R_m}$ for intense over-ocean TCs. Table 1 lists the regressed coefficient for the four rainfall distribution parameters in the present climate and future climate. The increase in $\overline{T_m}$ under warming is attributed to the increases of intercept value (a_1), slope (b_1), and $TCW\,\frac{V_{\max_{850}}}{R_{\mathrm{mw}_{850}}}$. To separate the effects of increased intercept, slope, and $TCW\,\frac{V_{\max_{850}}}{R_{\mathrm{mw}_{850}}}$, the $\overline{T_m}$ change caused by each individual factor is calculated. The increases of $TCW\,\frac{V_{\max_{850}}}{R_{\mathrm{mw}_{850}}}$, intercept, and slope contribute to the increase of $\overline{T_m}$ at 75.49%, 12.90%, and 9.26% respectively.

The mean $TCW\,\frac{V_{\max_{850}}}{R_{\mathrm{mw}_{850}}}$ increases by 21.60% (9.56%/K) in the future climate and is the dominant factor leading to the $\overline{T_m}$ increase. Following the idea of moisture decomposition in Shi and Durran (2015), the increase of $TCW\,\frac{V_{\max_{850}}}{R_{\mathrm{mw}_{850}}}$ can be further decomposed into the dynamic contribution and thermodynamic contribution.

$$\left[\delta\left(TCW\,\frac{V_{\max_{850}}}{R_{\mathrm{mw}_{850}}}\right)\right]_{\mathrm{dyna}} = \overline{TCW}\;\delta\left(\frac{V_{\max_{850}}}{R_{\mathrm{mw}_{850}}}\right), \tag{5a}$$

$$\left[\delta\left(TCW\,\frac{V_{\max_{850}}}{R_{\mathrm{mw}_{850}}}\right)\right]_{\mathrm{ther}} = \overline{\frac{V_{\max_{850}}}{R_{\mathrm{mw}_{850}}}}\;\delta(TCW), \tag{5b}$$

where $\overline{TCW}$, $\overline{\frac{V_{\max_{850}}}{R_{\mathrm{mw}_{850}}}}$ represent the mean TCW, $\frac{V_{\max_{850}}}{R_{\mathrm{mw}_{850}}}$ between present climate and future climate respectively; δ represents the difference between present and future climates. The dynamic contribution is related to the change in $\frac{V_{\max_{850}}}{R_{\mathrm{mw}_{850}}}$, and the thermodynamic contribution is related to the change in TCW. The increase in $TCW\,\frac{V_{\max_{850}}}{R_{\mathrm{mw}_{850}}}$ is dominantly from the thermodynamic contribution at 82.53%. In contrast, the dynamic contribution only accounts for 9.81%. Therefore, the increase in $\overline{T_m}$ is primarily due to the increase in atmospheric moisture. This is consistent with previous studies (Stansfield & Reed, 2023) suggesting that the increase in extreme TC precipitation rate under warming is mainly from the increase of atmospheric moisture.

The intercept value a_1 implies the background $\overline{T_m}$ in the absence of cyclones. Under warming, the a_1 value increases by 6.03% (2.67%/K). This value is less than the C-C scaling, which is reasonable because the background rainfall corresponds to a non-extreme precipitation scenario. The non-extreme precipitation typically increases at a rate smaller than the C-C scaling (e.g., Chen & Shi, 2023).

The slope b_1, reflecting the sensitivity of T_m to $TCW\,\frac{V_{\max_{850}}}{R_{\mathrm{mw}_{850}}}$, increases slightly by 2.59% (1.15%/K) in the future climate. In contrast, PHRaMM's regression coefficient for $V_{\max_{10m}}$ surges by 79.41% (35.14%/K), challenging Kim et al. (2022)'s assumption of constant sensitivity of T_m to TC intensity under warming and suggesting a nonlinear relationship between the TC inner core rain rates and the TC intensity. This nonlinearity likely originates from elevated background moisture levels under warming, which provides TCs with a greater reservoir of condensable water, amplifying rainfall production, particularly in the inner core where intense convergence are most pronounced. We found TCW rises by 17.59% (7.78%/K) in this study. Unlike PHRaMM, which treats cyclone dynamics and moisture as independent, the PHRaM_S captures their interactive effects via $TCW\,\frac{V_{\max_{850}}}{R_{\mathrm{mw}_{850}}}$ yielding a more stable scaling with T_m. The sensitivity of T_m to $\frac{V_{\max_{850}}}{R_{\mathrm{mw}_{850}}}$, without moisture component, increases by 24.99%

(11.06%/K) in the future climate. This heightened sensitivity (compared to b_1) suggests that unaccounted moisture effects substantially accelerate the rainfall maximum increase with TC intensity under warming.

Similar to $\overline{T_m}$, the increase in $\overline{T_o}$ is dominantly from the increase in $TCW\,\frac{V_{\max_{850}}}{R_{\mathrm{mw}_{850}}}$ at 60.48%. R_e is parameterized by $R_{\mathrm{mw}_{850}}$, and the decreased $\overline{R_e}$ is attributed to the decrease in slope b_3 and $R_{\mathrm{mw}_{850}}$. The mean $R_{\mathrm{mw}_{850}}$ decreases slightly by 2.89% (1.28%/K) in the future climate. The decrease in $R_{\mathrm{mw}_{850}}$ dominates the decrease of $\overline{R_e}$, accounting for 81.60%. The intercept (b_3) and slope (a_3) changes account for -15.83% and 36.56% respectively for the $\overline{R_e}$ decrease. The R_m values are at 25 km grid spacing, leading to difficulties in their predictions. R_m is predicted by $V_{\max_{850}}$ and the $\overline{R_m}$ decreases slightly from 31.15 to 30.42 km. The $\overline{R_m}$ shrinking is not well interpreted by the regression model since the intercept and slope change significantly in different climates (Table 1). The 25 km grid resolution limits the capture of R_m, resulting in R_m values being narrowly distributed across a few discrete values, especially for the intense TCs that we focus on.

6. Discussions and Conclusions

GCMs have been extensively utilized to explore TC rainfall patterns under warming, yet many previous studies focus on statistical summaries rather than the physical mechanisms driving rainfall patterns. This is likely due to the coarse resolutions of GCMs, which struggle to resolve vertical motions and inner-core dynamics. In this study, we fill the gaps by investigating shifts and physical drivers of four key rainfall distribution parameters—rainfall at the TC center (T_o), maximum rainfall (T_m), maximum rainfall radius (R_m), and e-folding radius (R_e)—critical to describing the radial rainfall field, using the MRI HighRes CMIP6 simulation. We find mean T_m and T_o ($\overline{T_m}$ and $\overline{T_o}$) increase by 8.65%/K and 8.86%/K, respectively, driven primarily by thermodynamic effects (enhanced moisture), while mean R_m and R_e ($\overline{R_m}$ and $\overline{R_e}$) decrease by 1.03%/K and 1.79%/K, reflecting a more compact rainfall structure tied to a shrinking inner core.

This study also highlights a nonlinear relationship between TC intensity and inner-core precipitation under warming, where moisture amplifies sensitivity. The scaling of T_m with $V_{\max_{10m}}$ rises sharply (35.14%/K), challenging assumptions of constant sensitivity (e.g., Kim et al., 2022). Additionally, T_m strongly correlates $(r = 0.8)$ with a moisture convergence proxy $\left(TCW\,\frac{V_{\max_{850}}}{R_{\mathrm{mw}_{850}}}\right)$, with 850 hPa variables showing significantly stronger correlations than surface metrics, suggesting TC circulation is better captured at the boundary layer top. This scaling with the moisture convergence proxy remains consistent across climates and TC categories, highlighting its reliability. These findings have implications for developing statistical TC rainfall models, particularly in how moisture and dynamic components are treated. The independent consideration of the moisture component (e.g., humidity) and the dynamic component (e.g., wind, vorticity) may lead to significant variations in the regressed coefficients. Using variables at 850 hPa, in the lower troposphere just above the boundary layer, instead of surface metrics could improve model accuracy by better capturing TC circulation and its interactions with moisture.

Despite its 25 km resolution—advanced for GCMs (Roberts et al., 2020)—the MRI data set has limitations. It cannot resolve TC eyes or distinct outer rainbands, potentially skewing T_o and T_m. Furthermore, Davis (2018) highlights that 25 km grids cannot accurately simulate Category 4 and 5 TCs—prevalent in our study—without errors in storm size, affecting both wind fields and related rainfall metrics like R_m and R_e. Reliance on a single model also limits generalizability, as TC rainfall structures vary across GCMs (Moon et al., 2022). We stress that our results are specific to this simulation and require cautious interpretation. Future studies with <10 km resolution could improve parameter estimates. Despite these constraints, our framework—analyzing wind-rain relationships, developing parameterized models for key rainfall parameters, and interpreting parameter changes—can be extended to other high-resolution models, offering a pathway to further explore TC rainfall dynamics across diverse climate simulations.

Data Availability Statement

TempestExtremes software is available at Ullrich et al. (2024). The MRI HighRes CMIP6 data is available at Mizuta et al. (2019).

Acknowledgments

The work is substantially supported by a grant from the Research Grants Council (RGC) of the Hong Kong Special Administrative Region, China (Project Reference Number: AoE/P-601/23-N). Additionally, JC and XS receive support from RGC Grant T31-603/21-N and HKUST-16307323, while JC and DX are supported by an HKU start-up fund 000250348.130087.25300.100.01.

References

Chen, J., & Shi, X. (2023). Quantifying global warming response of the orographic precipitation in a typhoon environment with large-eddy simulations. *Journal of Climate*, *36*(19), 6951–6966. https://doi.org/10.1175/JCLI-D-23-0018.1

Davis, C. (2018). Resolving tropical cyclone intensity in models. *Geophysical Research Letters*, *45*(4), 2082–2087. https://doi.org/10.1002/2017GL076966

Emanuel, K. (2018). 100 years of progress in tropical cyclone research. *Meteorological Monographs*, *59*, 15–21. https://doi.org/10.1175/AMSMONOGRAPHS-D-18-0016.1

He, J., Brogniez, H., & Picon, L. (2022). Evaluation of tropical water vapour from CMIP6 global climate models using the ESA CCI Water Vapour climate data records. *Atmospheric Chemistry and Physics*, *22*(18), 12591–12606. https://doi.org/10.5194/acp-22-12591-2022

Kim, D., Park, D.-S. R., Nam, C. C., & Bell, M. M. (2022). The parametric hurricane rainfall model with moisture and its application to climate change projections. *npj Climate and Atmospheric Science*, *5*(1), 86. https://doi.org/10.1038/s41612-022-00308-9

Knapp, K. R., Kruk, M. C., Levinson, D. H., Diamond, H. J., & Neumann, C. J. (2010). The international best track archive for climate stewardship (IBTrACS) unifying tropical cyclone data. *Bulletin of the American Meteorological Society*, *91*(3), 363–376. https://doi.org/10.1175/2009BAMS2755.1

Knutson, T., Camargo, S. J., Chan, J. C. L., Emanuel, K., Ho, C.-H., Kossin, J., et al. (2020). Tropical cyclones and climate change assessment: Part II: Projected response to anthropogenic warming. *Bulletin of the American Meteorological Society*, *101*(3), E303–E322. https://doi.org/10.1175/BAMS-D-18-0194.1

Liu, M., Vecchi, G. A., Smith, J. A., & Knutson, T. R. (2019). Causes of large projected increases in hurricane precipitation rates with global warming. *npj Climate and Atmospheric Science*, *2*(1), 38. https://doi.org/10.1038/s41612-019-0095-3

Lonfat, M., Marks, F. D., & Chen, S. S. (2004). Precipitation distribution in tropical cyclones using the tropical rainfall measuring mission (TRMM) microwave imager: A global perspective. *Monthly Weather Review*, *132*(7), 1645–1660. https://doi.org/10.1175/1520-0493(2004)132⟨1645:PDITCU⟩2.0.CO;2

Lonfat, M., Rogers, R., Marchok, T., & Marks, F. D. (2007). A parametric model for predicting hurricane rainfall. *Monthly Weather Review*, *135*(9), 3086–3097. https://doi.org/10.1175/MWR3433.1

Mizuta, R., Yoshimura, H., Ose, T., Hosaka, M., & Yukimoto, S. (2019). MRI MRI-AGCM3-2-S model output prepared for CMIP6 HighResMIP highresSST-future. (Version 20240301) [Dataset]. *Earth System Grid Federation*. https://doi.org/10.22033/ESGF/CMIP6.6740

Moon, Y., Kim, D., Wing, A. A., Camargo, S. J., Zhao, M., Leung, L. R., et al. (2022). An evaluation of tropical cyclone rainfall structures in the HighResMIP simulations against satellite observations. *Journal of Climate*, *35*(22), 7315–7338. https://doi.org/10.1175/jcli-d-21-0564.1

Roberts, M. J., Camp, J., Seddon, J., Vidale, P. L., Hodges, K., Vannière, B., et al. (2020). Projected future changes in tropical cyclones using the CMIP6 HighResMIP multimodel ensemble. *Geophysical Research Letters*, *12*(14), e2020GL088662. https://doi.org/10.1029/2020gl088662

Shi, X., & Durran, D. R. (2015). Estimating the response of extreme precipitation over midlatitude mountains to global warming. *Journal of Climate*, *28*(10), 4246–4262. https://doi.org/10.1175/JCLI-D-14-00750.1

Shi, X., Liu, Y., Chen, J., Chen, H., Wang, Y., Lu, Z., et al. (2024). Escalating tropical cyclone precipitation extremes and landslide hazards in South China under Global Warming. *npj Climate and Atmospheric Science*, *7*(1), 107. https://doi.org/10.1038/s41612-024-00654-w

Stansfield, A. M., & Reed, K. A. (2023). Global tropical cyclone precipitation scaling with sea surface temperature. *npj Climate and Atmospheric Science*, *6*(1), 60. https://doi.org/10.1038/s41612-023-00391-6

Tu, S., Xu, J., Chan, J. C. L., Huang, K., Xu, F., & Chiu, L. S. (2021). Recent global decrease in the inner-core rain rate of tropical cyclones. *Nature Communications*, *12*(1), 1948. https://doi.org/10.1038/s41467-021-22304-y

Tuleya, R. E., DeMaria, M., & Kuligowski, R. J. (2007). Evaluation of GFDL and simple statistical model rainfall forecasts for U.S. landfalling tropical storms. *Weather and Forecasting*, *22*(1), 56–70. https://doi.org/10.1175/WAF972.1

Ullrich, P., Zarzycki, C. M., McClenny, E. E., Pinheiro, M. C., Stansfield, A. M., & Reed, K. A. (2021). TempestExtremes v2.1: A community framework for feature detection, tracking, and analysis in large datasets. *Geoscientific Model Development*, *14*(8), 5023–5048. https://doi.org/10.5194/gmd-14-5023-2021

Ullrich, P., Zarzycki, C. M., McClenny, E. E., Pinheiro, M. C., Stansfield, A. M., & Reed, K. A. (2024). Tempestextremes [Software]. *Github*. Retrieved from https://github.com/ClimateGlobalChange/tempestextremes

Xi, D., & Lin, N. (2022). Investigating the physical drivers for the increasing tropical cyclone rainfall hazard in the United States. *Geophysical Research Letters*, *49*(15), e2022GL099196. https://doi.org/10.1029/2022GL099196

Xi, D., Wang, S., & Lin, N. (2022). Analyzing relationships between tropical cyclone intensity and rain rate over the ocean using numerical simulations. *Journal of Climate*, *36*, 1–24. https://doi.org/10.1175/JCLI-D-22-0141.1

Yu, Z., Wang, Y., Yu, H., & Duan, Y. (2022). The relationship between the inner-core size and the rainfall distribution in landfalling tropical cyclones over China. *Geophysical Research Letters*, *49*(8), e2021GL097576. https://doi.org/10.1029/2021GL097576